# Monitoring Subglacial Volcanic Eruption Using Ground-Based C-Band Radar Imagery

Frank Silvio Marzano, *Senior Member, IEEE*, Stefano Barbieri, Errico Picciotti, and Sigrùn Karlsdóttir

***Abstract*—The microphysical and dynamical features of volcanic clouds, due to Plinian and sub-Plinian eruptions, can be quantitatively monitored by using ground-based microwave weather radars. In order to demonstrate the unique potential of this remote sensing technique, a case study of a subglacial volcanic eruption, occurred in Iceland in November 2004, is described and analyzed. Volume data, acquired by a C-band ground-based weather radar, are processed to automatically classify and estimate ash particle concentration. The ash retrieval physical–statistical algorithm is based on a backscattering microphysical model of fine, coarse, and lapilli ash particles, used within a Bayesian classification and optimal regression algorithm. A sensitivity analysis is carried out to evaluate the overall error budget and the possible impact of nonprecipitating liquid and ice cloud droplets when mixed with ash particles. The evolution of the Icelandic eruption is discussed in terms of radar measurements and products, pointing out the unique features, the current limitations, and future improvements of radar remote sensing of volcanic plumes.**

***Index Terms*—Ash retrieval, inversion methods, microwave weather radars, radar meteorology, volcanic eruption clouds.**

## I. Introduction

ASH dispersal from large explosive volcanic eruptions is very extensive and can be devastating for the environment, endangering people's lives and property [1]. In addition, volcanoes influence the global climate on timescales of years. During a Plinian or sub-Plinian eruption, the injection of large amounts of fine and coarse rock fragments and corrosive gases into the troposphere and lower stratosphere is usually followed by a long lasting ashfall which can cause a variety of damages [2]–[5]. Volcanic ash clouds are an increasing hazard to aviation safety because of growing airline traffic [6], [7].

Manuscript received June 3, 2008; revised March 2, 2009 and April 20, 2009. First published September 15, 2009; current version published December 23, 2009. This work was supported in part by the University "La Sapienza" of Rome, Rome, Italy, and in part by the Italian Department of Civil Protection, Rome, Italy.

F. S. Marzano and S. Barbieri are with the Department of Electronic Engineering, University "La Sapienza" of Rome, 00184 Rome, Italy, and also with the Centro di Eccellenza per l'integrazione di Tecniche di Telerilevamento e Modellistica Numerica per la Previsione di Eventi Meteorologici Severi (CETEMPS), University of L'Aquila, Via Vetoio, 67010 L'Aquila, Italy (e-mail: marzano@die.uniroma1.it; stefano.barbieri@inwind.it).

E. Picciotti was with CETEMPS, University of L'Aquila, 67010 L'Aquila, Italy. He is now with the Radar Meteorology Division, HIMET, 67100 L'Aquila, Italy (e-mail: errico.picciotti@himet.it).

S. Karlsdóttir is with the Icelandic Meteorological Office, 150 Reykjavík, Iceland (e-mail: sigk@vedur.is).

Color versions of one or more of the figures in this paper are available online at http://ieeexplore.ieee.org.

Digital Object Identifier 10.1109/TGRS.2009.2024933

The real-time and areal monitoring of a volcano eruption, in terms of its intensity and dynamics, is not always possible by conventional visual inspections. Remote sensing techniques both from ground and space represent unique tools to be exploited [8]–[10]. In particular, microwave weather radars can gather 3-D information of atmospheric ash-cloud scattering volumes up to several hundreds of kilometers, in all weather conditions, at a fairly high spatial resolution (less than a kilometer) and with a repetition cycle of few minutes [11]–[15]. Single-polarization Doppler radars can measure horizontally polarized power echo and Doppler shift from which ash content and radial velocity can be, in principle, extracted. In spite of these potentials, there are still several open issues about microwave weather radar capabilities to detect and quantitatively retrieve ash-cloud parameters [14], [15].

Several unknowns may condition the accuracy of radar products, most of them related to microphysical variability of ash clouds due to particle size distribution (PSD), shape, and dielectric composition [16]. Ash aggregation with liquid and frozen hydrometeors is one of the most critical issues, as it is an effect difficult to discriminate and separate from radar observations [17]–[19]. A major impairment in the exploitation of microwave weather radars for volcanic eruption monitoring is due to the exclusive use of operational weather radars for clouds and precipitation observation and to the few available case studies during which a weather radar is operating during an explosive volcanic eruption.

Previous works were devoted to the modeling of the radar reflectivity response due to volcanic ash clouds and to the design of a volcanic ash radar retrieval (VARR) methodology able to provide both ash concentration and fall rates from a radar polar scan in an automatic fashion [15], [16]. The aims of this paper are twofold: 1) to extend the sensitivity analysis of VARR and evaluate its overall error budget by including the possible impact of nonprecipitating liquid and ice cloud droplets when mixed with ash particles and 2) to illustrate the potential of VARR through a detailed discussion of a case study of a subglacial volcanic eruption, occurred in Iceland in November 2004 and observed by a single-polarization weather radar at 5.6 GHz [20]. The evolution of the Icelandic eruption is discussed in terms of radar measurements and retrievals, pointing out the unique features and the current limitations of radar remote sensing of volcanic plumes.

This paper is organized as follows. In Section II, we will describe the numerical sensitivity analysis with respect to particle combination within ash clouds and summarize the overall radar retrieval algorithm with some improvements. In Section III, the

subglacial volcanic eruption will be illustrated in terms of radar imagery and products. Section IV will draw some conclusions and future perspectives.

## II. Retrieval Approach and Sensitivity Analysis

A microwave weather radar response is mainly controlled by the atmospheric PSD within the range volume bin. In the case of ash-cloud formation processes within a humid environment, we may suppose to have two distinct particle-combination phenomena within an observed range volume: 1) coexistence of ash particle and hydrometeors without mixing processes and 2) aggregation (or mixture) of ash particles with hydrometeors to form a new mixed-phase particle [17]–[19].

The goal of the next sections is to evaluate the impact of nonprecipitating hydrometeors on ash-cloud radar signatures at C-band and to assess the overall error budget for the ash retrieval.

### A. Impact of Particle Combination on Radar Reflectivity

In order to take into account the hydrometeor effect, we have considered the following categories of ash particle ($p = a$): fine ash, coarse ash, and lapilli. For hydrometeor particles ($p = h$), we have concentrated our attention on cloud ice and water droplets, due to the subglacial winter eruption here studied. On the other hand, precipitating hydrometeors, such raindrops, graupel, and snow, should exert a sort of atmospheric scrubbing, thus removing and/or obscuring ash signatures. There is a fairly large consensus about the capability to model PSD through either a normalized Gamma or Weibull size distribution [2], [16]. In the case of a multimode size distribution, it is always possible to suppose more than one analytical PSD characterized by different mean sizes and total number of particles.

In this paper, we have adopted the scaled Gamma (SG) PSD as a general model both for ash and hydrometeor particles (the results can be easily extended to a Weibull PSD). The SG PSD $N_p$ for a generic class of particles $p$ can be written as [16]

$$N_p(D) = N_{np}\left(\frac{D}{D_{np}}\right)^{\mu_p} e^{-\Lambda_{np}\left(\frac{D}{D_{np}}\right)} \tag{1}$$

where $D$ is the diameter (in millimeters), and the "intercept" parameter $N_{np}$ and the "slope" parameter $\Lambda_{np}$ in a logarithmic plane are related to the PSD "shape" parameter $\mu_p$ through

$$\begin{cases} N_{np} = 10^6 \frac{6C_p\Lambda_{np}^{\mu_p+4}}{\pi\rho_p D_{np}^4 \Gamma(\mu_p+4)} \\ \Lambda_{np} = \mu_p + 1 \end{cases} \tag{2}$$

with $C_p$ being the mass concentration (in $\mathrm{g}\cdot\mathrm{m}^{-3}$), $\rho_p$ the specific density (in kilograms per cubic meter), and $D_{np}$ the mean diameter (in millimeters). It is worth mentioning that $N_{np}$ has a dimension which is $\mu_p$-independent and given in units per millimeter per cubic meter, $\Lambda_{np}$ is adimensional, and $N_p(D)$ is completely specified by the three parameters $\mu_p$, $D_{np}$, and $C_p$ (assuming a constant density $\rho_p$).

Let us assume the following: 1) Particles are spherical or equivalently spherical so that their mass is $M_p = \rho_p(\pi/6)D^3$ with a constant specific density $\rho_p$ and 2) the minimum and maximum diameters are zero and infinite so that the complete moment $m_{lp}$ of order $l$ of $N_p(D)$ is expressed by

$$m_{lp} = \frac{N_{np}}{\Lambda_{np}^{l+\mu_p+1}} D_{np}^{l+1}\Gamma(l+\mu_p+1) \tag{3}$$

where $\Gamma(l+1) = l!$ if $l$ is an integer. Then, the total volumetric number of particles is $N_{tp} = m_{0p}$, whereas the *mass concentration* $C_p$ is given by

$$C_p = (\pi/6)\rho_p \int_0^\infty D^3 N_p(D)\, dD = \frac{\pi}{6}\rho_p m_{3p} \tag{4}$$

and the *number-weighted mean diameter* $D_{np}$ is defined by

$$D_{np} = \frac{\int_0^\infty D N_p(D)\, dD}{\int_0^\infty N_p(D)\, dD} = \frac{m_{1p}}{m_{0p}}. \tag{5}$$

Note that from (1), (4), and (5), we can simply derived the relationships in (2).

The particle fall flux $R_p$, defined as the particle mass crossing a horizontal cross section of unit area over a given interval of time, can be expressed by the following:

$$R_p = (\pi/6)\rho_p \int_0^\infty \left[\nu_p(D) - w_u\right] D^3 N_p(D)\, dD \tag{6}$$

where $\nu_p(D)$ is the particle downward terminal fall velocity (in meters per second) in still air, and $w_u$ is the upward vertical component of the air speed. In (6), $R_p$ is measured in kilograms per square meter per steradin, but if it is divided by the specific density $\rho_p$, then it is expressed in meters per second, thus expressing a particle fall rate.

The mean diameters $D_{na}$ of ash particles are set to 0.01, 0.1, and 1.0 mm for fine, coarse, and lapilli, respectively [15]. For all ash classes, the density $\rho_a$ is put equal to 1800 $\mathrm{kg/m^3}$, whereas the shape parameter $\mu_a$ is varied between one and two. For the hydrometeor particle, the mean diameters $D_{nh}$ are set to 0.01 mm for both cloud ice and water particles. Their density $\rho_h$ is put equal to 1000 $\mathrm{kg/m^3}$ for water and 900 $\mathrm{kg/m^3}$ for ice, whereas the shape parameter $\mu_h$ is varied between 3 and 16 for both cloud droplets [19], [21].

Microwave scattering from ash particles and from cloud water and ice droplets satisfies the Rayleigh approximation. Under this condition, the radar reflectivity factor at horizontal polarization $Z_{\mathrm{Hp}}$, expressed in $\mathrm{mm^6\cdot m^{-3}}$, due to an ensemble of particles $p$, is expressed as the sixth moment of PSD as follows [16], [22]:

$$Z_{\mathrm{Hp}} = \eta_{\mathrm{Hp}} \frac{\lambda^4}{\pi^5 |K_p|^2} = \int_0^\infty D^6 N_p(D)\, dD = m_{6p} \tag{7}$$

where $\eta_{\mathrm{Hp}}$ is the radar volumetric reflectivity, $\lambda$ is the wavelength, and $K_p$ is the dielectric factor of the particle ensemble

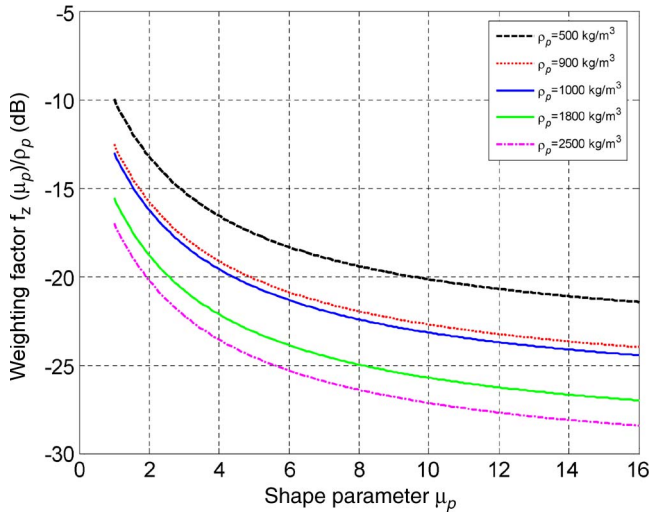


Fig. 1. Weighting factor $f_Z$, normalized to particle density $\rho_p$, versus the shape parameter $\mu_p$ (with values between 1 and 16), characterizing the PSD. Particle specific densities between 500 and 2500 kg/m$^3$ are used as parameter (with ice at 900 kg/m$^3$ and water at 1000 kg/m$^3$).

of category $p$. For brevity, hereinafter, the term radar reflectivity will also stand for radar reflectivity factor. Substituting (3) in (7), we obtain

$$Z_{\mathrm{Hp}} = \frac{N_{np}}{\Lambda_{np}^{\mu_p+7}} D_{np}^7 \Gamma(\mu_p + 7). \tag{8}$$

Using (2), the latter equation yields

$$Z_{\mathrm{Hp}} = f_Z(\mu_p) \frac{C_p}{\rho_p} D_{np}^3 \tag{9}$$

where $Z_{\mathrm{Hp}}$ is expressed in mm$^6 \cdot$ m$^{-3}$, and $f_Z$ is a *weighting* function of $\mu_p$ only, given by

$$f_Z(\mu_p) = \frac{6 \cdot 10^6}{\pi(\mu_p+1)^3} \frac{\Gamma(\mu_p+7)}{\Gamma(\mu_p+4)}. \tag{10}$$

The parametric plot of the normalized weighting factor $f_Z/\rho_p$ is shown in Fig. 1 as a function of the shape parameter $\mu_p$. For the increasing values of $\mu_p$ and $\rho_p$, Fig. 1 suggests that the normalized weighting factor in (9) decreases.

Two particle-combination models are here considered: coexistence and mixture [18]. If we suppose ***coexistence*** of ash and cloud particles within the radar resolution volume, the two particle categories do not mix to each other and remain physically separated. Thus, the total reflectivity $Z_{Hcoe}$ is the sum of the respective reflectivities due to ash particle $(p = a)$ $Z_{Ha}$ and to the hydrometeor particles $(p = h)$ $Z_{Hh}$ as follows:

$$\begin{aligned} Z_{Hcoe} &= Z_{Ha} + Z_{Hh} \\ &= f_Z(\mu_a) \frac{C_a}{\rho_a} D_{na}^3 + f_Z(\mu_h) \frac{C_h}{\rho_h} D_{nh}^3. \end{aligned} \tag{11}$$

In the case of a ***mixture*** of ash and hydrometeor particles, we can suppose an aggregation microphysical process which leads to a new particle having different PSDs and concentrations [17]. Aggregation microphysical processes leading to mixtures are quite complicated and are generally described by diagnostic differential equations [19], whose description is beyond this paper. However, from a radar perspective, if we assume the radar resolution volume to be completely filled by this particle mixture $(p = m)$, the total reflectivity $Z_{H\mathrm{mix}}$ due to the particle mixture can be expressed by

$$Z_{H\mathrm{mix}} = f_Z(\mu_m) \frac{C_m}{\rho_m} D_{nm}^3 \tag{12}$$

where $C_m = C_a + C_h$ is the mixture concentration. The parameters in (12) can be, in general, modeled as a weighted average of the ash and droplet respective parameters [19]. In particular, we can define the mixture characteristic radius as

$$D_{nm} = \frac{C_a D_{na} + C_h D_{nh}}{C_a + C_h}. \tag{13}$$

In the absence of detailed microphysical models, the PSD shape parameter $\mu_m$ of the particle mixture can be also expressed by [19]

$$\mu_m = \frac{C_a \mu_a + C_h \mu_h}{C_a + C_h}. \tag{14}$$

Note that the dielectric factor $K_m$ of the particle mixture [see (7)] can be also modeled as $\mu_m$ by substituting in (14) $\mu_a$ with $K_a$ (equal to about 0.39) and $\mu_h$ with $K_h$ (equal to about 0.93) [16]. The density $\rho_m$ of particle mixture is obtained from the volume ratio of ash and water particles [19]

$$\rho_m = \frac{C_a + C_h}{C_a/\rho_a + C_h/\rho_h}. \tag{15}$$

We can investigate the sensitivity of radar response to the presence of nonprecipitating hydrometeors, using the coexistence and mixture microphysical models expressed in (11) and (12), respectively. To this purpose, we can express the particle concentration $C_p$ as a linear fraction of the total concentration $C_{\mathrm{tot}}$. If $f_h$ is the concentration fraction of hydrometeors within the radar volume bin, we can define the following simple models:

$$\begin{cases} C_a = (1 - f_h) C_{\mathrm{tot}} \\ C_h = f_h C_{\mathrm{tot}} \\ C_m = C_a + C_h = (1 - f_h) C_{\mathrm{tot}} + f_h C_{\mathrm{tot}} \end{cases} \tag{16}$$

with the fraction $f_h$ varying between zero (i.e., $C_{\mathrm{tot}} = C_a$ in the case of no hydrometeors) to one (i.e., $C_{\mathrm{tot}} = C_h$ in the case of no ash). The previous formula basically assumes a total mass conservation within the resolution volume: This means a redistribution of the total concentration $C_{\mathrm{tot}}$ with respect to ash and hydrometeor fractions.

The following figures show some numerical results obtained from the previous models. For the case of coexistence mechanism, Fig. 2 shows the radar reflectivity factor $Z_{Hcoe}$ as a function of $C_{\mathrm{tot}}$ for the coexistence of fine, coarse, and lapilli ashes with cloud water and ice droplets for various hydrometeor fractions $f_h$. The variability of $C_{\mathrm{tot}}$ within (16) is between 0.1 and 10 g/m$^3$, whereas $\mu_a = 1$ and $\mu_h = 5$ have been assumed. Fig. 3 shows the same as Fig. 2, but for the radar reflectivity factor $Z_{H\mathrm{mix}}$ (in dBZ) as a function of $C_{\mathrm{tot}}$ for the mixture of

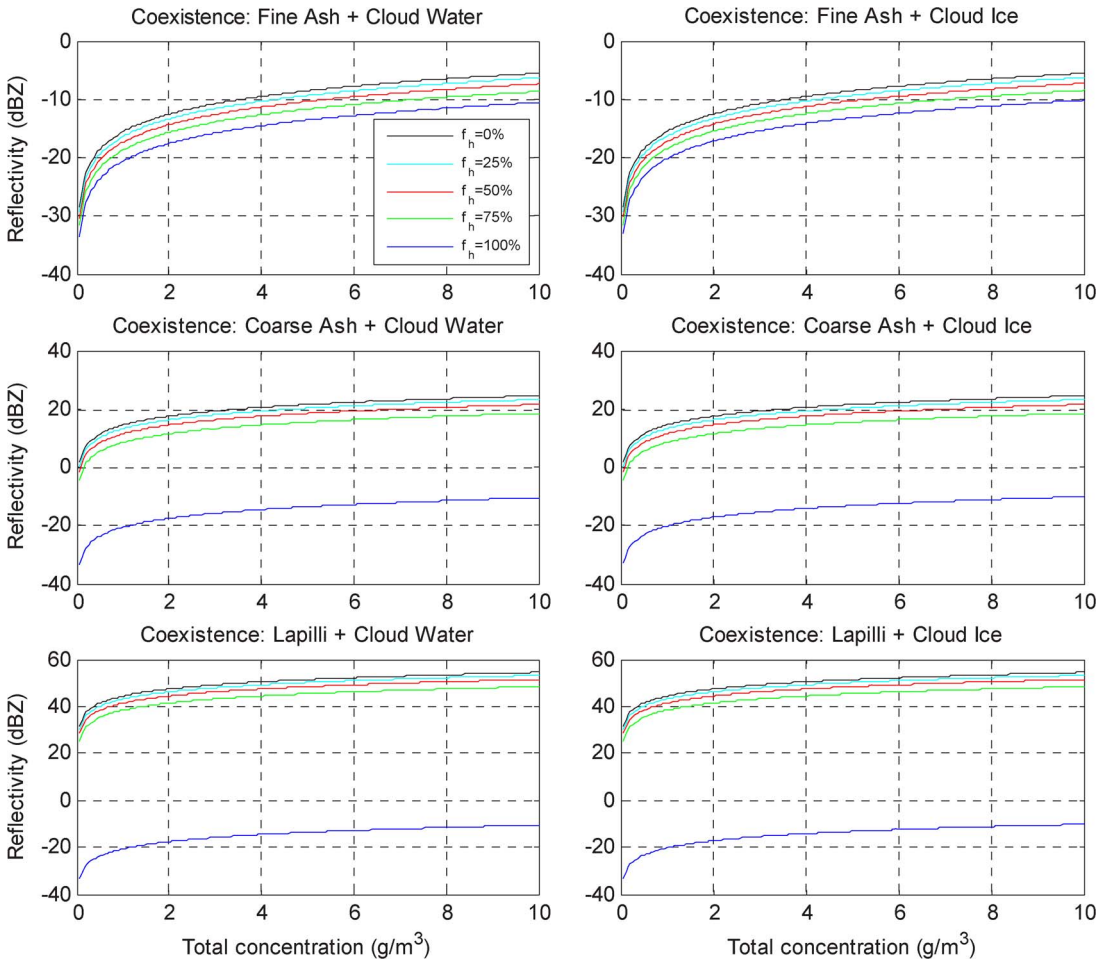


Fig. 2. Radar reflectivity as a function of total concentration considering the ***coexistence*** of ash particles with a percentage fraction $f_h$ of hydrometeors (assuming mass conservation). (Top panels) Fine ash coexistent with cloud water and cloud ice. (Middle panels) Coarse ash coexistent with cloud water and cloud ice. (Bottom panels) Lapilli coexistent with cloud water and cloud ice.

fine ash, coarse ash and lapilli with cloud water and ice droplets for various $f_h$'s.

Some significant features of combination process radar response can be derived from the analysis of Figs. 2 and 3 as follows.

1) It is evident that, for $f_h = 0$ and $f_h = 1$, $Z_{Hcoe} = Z_{H\mathrm{mix}}$ holds. This means that the two combination models, coexistence and mixture, modulate the reflectivity values between these two extremes.
2) Pure ice and pure water hydrometeors (i.e., $f_h = 1$) exhibit low reflectivities between $-30$ and $-10$ dBZ. These values can be partially explained by their small mean sizes (i.e., 0.01 mm), but it would not justify the smaller values with respect to pure fine ash with the same mean size. However, since we fixed $\mu_a = 1$ with $\rho_a = 1800$ kg/m$^3$ and $\mu_h = 5$ with $\rho_h = 1000$ or 900 kg/m$^3$, from Fig. 1, it is apparent that the normalized weighting factor is less for cloud hydrometeors (about $-22$ dB) than for fine-ash particles (about $-16$ dB). Note that, within this modeling framework, from (9), cloud ice reflectivity tends to be slightly greater than that of cloud water due to the slightly diverse specific density (causing a $Z_H$ difference of only 0.46 dB). However, the received power will be lower due to the fact that the dielectric factor $|K|^2 = 0.18$ for ice and $|K|^2 = 0.93$ for water (causing a difference of about 7.1 dB in terms of radar received power for the same PSD).
3) For a given total concentration, both coexistence and mixture tend to reduce the reflectivity due to pure ash. For a 50% coexistence, this reduction may be of few decibels for fine ash up to a maximum of 3 dB for lapilli. In the case of a 50% mixture, this reduction may double, going from 2 dB up to a maximum of 12 dB for lapilli. In general, for particle coexistence, the hydrometeor fraction tends to give less variability of reflectivity response when compared with that obtained from the mixture model.
4) Whereas the shape parameter $\mu_a$ of ash PSD is experimentally confined between one and two, the value $\mu_h$ for ice and water particles may range up 16 [19], [21]. From Fig. 1, we can deduce that the results of Figs. 2 and 3 will change when increasing $\mu_h$, showing a stronger reduction between pure ash and mixed cases due to the increase of $f_Z$ with $\mu_p$. This impact will be more pronounced for particle mixture than for coexistence. The decrease of $\mu_h$ with respect to the nominal value of five causes an opposite effect, of course.

In summary, the particle-combination processes, involving cloud liquid and frozen nonprecipitating particles within an ash

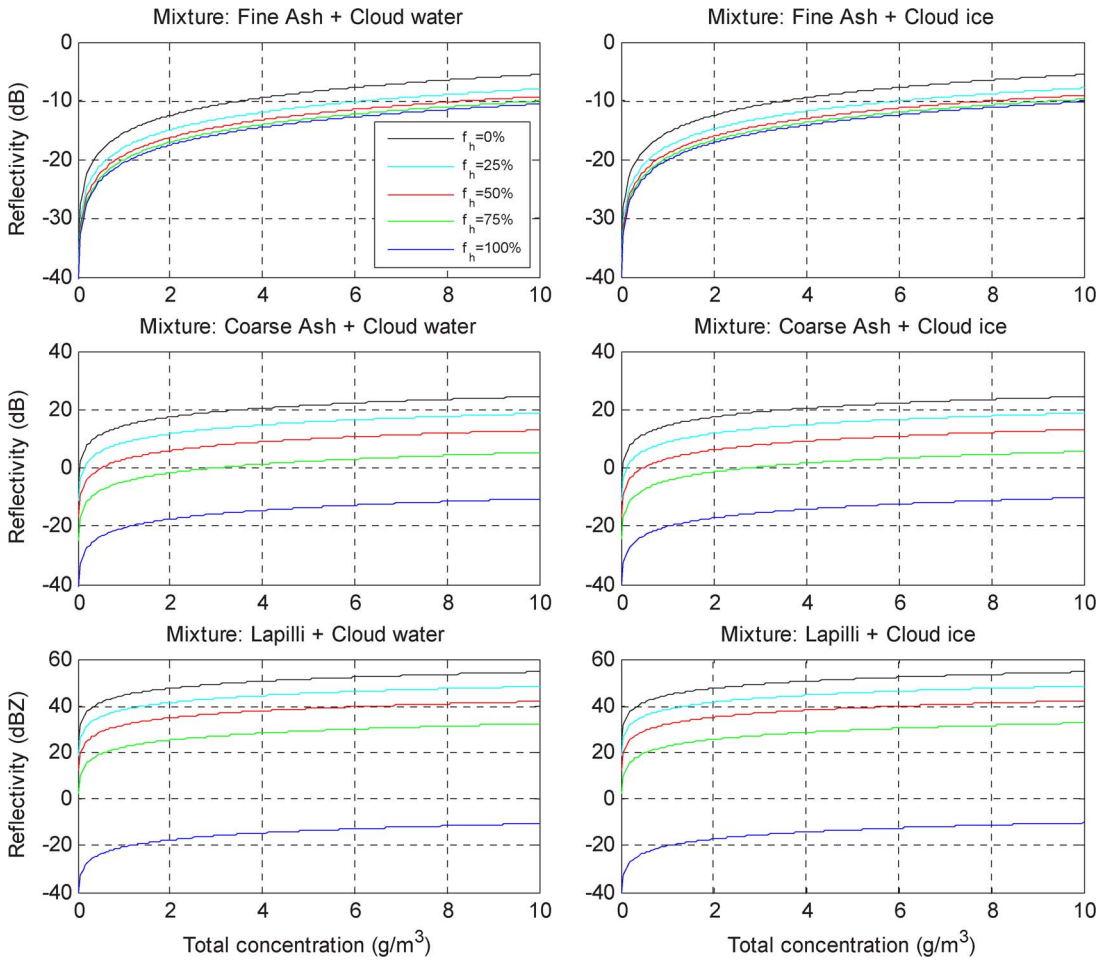


Fig. 3. Radar reflectivity as a function of total concentration considering the *aggregate* ***mixture*** of ash particles with a percentage fraction $f_h$ of hydrometeors (assuming mass conservation). (Top panels) Fine ash mixed with cloud water and cloud ice. (Middle panels) Coarse ash mixed with cloud water and cloud ice. (Bottom panels) Lapilli mixed with cloud water and cloud ice.

plume, tend to reduce the radar reflectivity signature in a way that they are dependent on the cloud particle distribution, ash mode, and aggregation process. For fine and coarse ashes within a fractional combination of 50%, the expected reflectivity reduction is generally less than 1 dB for coexistence and less than 5 dB for mixture with respect to the measured values.

### *B. Physically Based Ash Estimation Algorithm*

The retrieval of ash concentration $C_a$ and fall rate $R_a$ from the measured radar reflectivity $Z_{Hm}$ is a typical remote sensing inverse problem. The inverse problem can be stated as an estimation problem in a probabilistic framework [23]. A crucial role in this approach is played by the *a priori* information which consists of all knowledge about the geophysical solution, possibly translated as constraints within the inverse problem.

In our context, this means to construct an effective model of ash-cloud microphysics for remote sensing purposes [16]. As already mentioned, we have defined three classes (or modes) of ash sizes: fine ash, coarse ash, and lapilli [15]. As a synthesis of available volcanic information, within each class, we have supposed a Gaussian random distribution for [15] the following: 1) $D_{na}$ with average values $\langle D_{na} \rangle$ equal to 0.01, 0.1, and 1 mm for fine, coarse, and lapilli ashes and a standard deviation $\sigma_{Dn} = 0.2\langle D_{na} \rangle$ and 2) $C_a$ with mean values $\langle C_a \rangle$ equal to 0.1, 1, and 5 g/m$^3$ for light, moderate, and intense concentration regimes and a standard deviation $\sigma_{Ca} = 0.5\langle C_a \rangle$. Thus, the physically based VARR algorithm can be structured as follows: 1) the detection of one of the nine ash classes from the measured reflectivity $Z_{Hm}$ within each range bin by using a Bayesian identification technique and 2) the retrieval of the ash amount and fall rate for each class from the measured $Z_{Hm}$ by applying a polynomial regression method.

Since we do not have any chance to identify either coexistence or aggregation of ash and hydrometeors using single-polarization radar data only, we can take into account the effect of hydrometeors as a further uncertainty within the modeled noise. This is a conservative choice, but it is the only way to introduce this knowledge within our inversion algorithm, apart from possible *a priori* meteorological information. The modeled noise is added to the simulated reflectivity $Z_{Ha}$ of pure ash to reproduce the synthetic reflectivity measurement signatures $Z_{Hm}$. By introducing the random errors $\varepsilon_I$, $\varepsilon_M$, and $\varepsilon_A$ due to instrumental, modeling, and particle-combination uncertainties, respectively, we can express

$$Z_{Hm} = Z_{Ha} + \varepsilon_I + \varepsilon_M + \varepsilon_A \tag{17}$$

where all variables are in dBZ. The error sources may be ascribed to instrumental noise, modeled as a zero-mean Gaussian

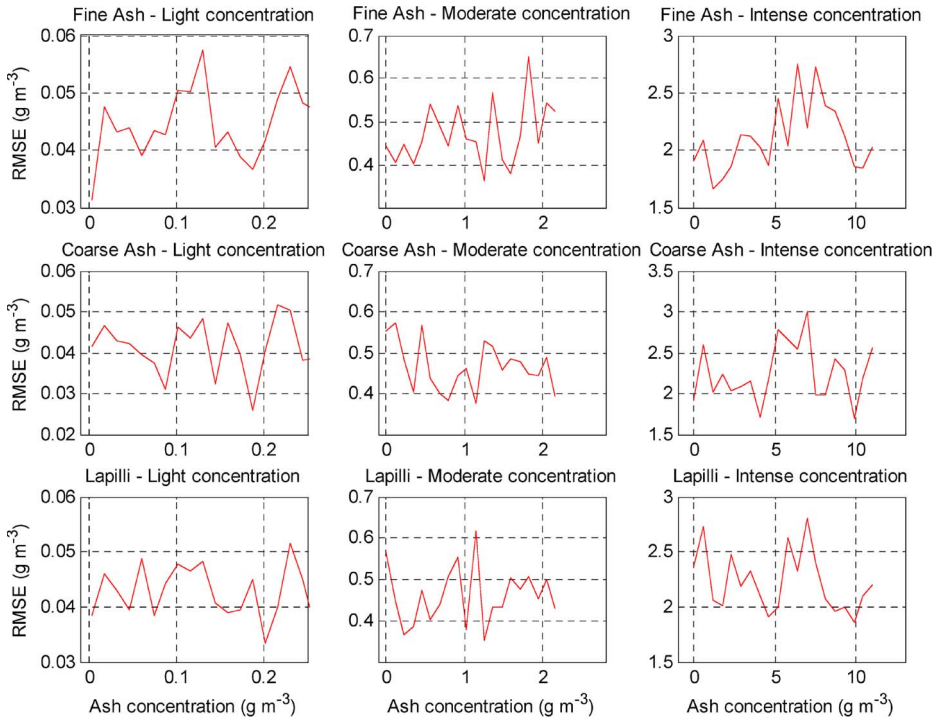


Fig. 4. Error structure of ash-concentration retrieval within each ash class, expressed in terms of rmse versus ash concentration. (Top panels) Fine ash. (Middle panels) Coarse ash. (Bottom panels) Lapilli.

error $\varepsilon_I$ with a standard deviation of 1 dBZ, and forward modeling uncertainties, modeled as a zero-mean Gaussian error $\varepsilon_M$ with a standard deviation of 1 dBZ. As previously shown, particle-combination effects can lead to an unknown underestimation of several decibels. A conservative choice is to assume $\varepsilon_A$ as a random error with a uniform distribution between 0 dBZ (no combination effects) and 5 dBZ (a compromise between coexistence and mixture underestimation maxima). The price to pay to design a robust inversion algorithm through (17) is to deal with a larger estimate error variance [23].

For what concerns the classification step, its aim is related to the possibility to automatically discriminate between ash categories which were defined as fine, coarse, and lapilli sizes. In the overall retrieval scheme, classification may represent a first qualitative output before performing parameter estimation. Maximum *a posteriori* probability criterion can be used to carry out cloud classification in a model-based supervised context. If $c$ is the ash class, then the conditional probability density function (pdf) of a class $c$ given a measurement $Z_{Hm}$ reduces to

$$\hat{c} = Mode\left[p(c|Z_{Hm})\right] \tag{18}$$

where $Mode$ is the modal value of the posterior pdf $p(c|Z_{Hm})$. Assuming a Gaussian probability framework to describe $p(c|Z_{Hm})$ and exploiting the Bayes theorem, computing (18) means to know the reflectivity mean $m_Z$ (also called class centroid) and standard deviation $\sigma_Z$ of $Z_{Hm}$ for each ash class $c$ [15]. The prior pdf can be used to subjectively weigh each class as a function of other available information.

Once an ash class is detected, then an estimate of ash concentration and fall rate is possible. A way to approach the quantitative retrieval problem is to adopt a statistical parametric model to describe the relation $X - Z_{Hm}$, where $X$ stands for either ash concentration $C_a$ or ashfall rate $R_a$ [15]. Assuming a power-law model, we can write the estimated quantity for each class $c$ as

$$\begin{cases} \hat{C}_a^{(c)} = \alpha[Z_{H_m}]^{\beta} \\ \hat{R}_a^{(c)} = \gamma[Z_{H_m}]^{\delta} \end{cases} \tag{19}$$

where the "hat" indicates the estimated quantity, whereas $\alpha$, $\beta$, $\gamma$, and $\delta$ are the class-dependent regression coefficients.

Fig. 4 shows the overall error budget for the ash-concentration estimation for all nine ash classes using the reflectivity model given in (17). The error, expressed in terms of root mean square (rms) value, is plotted with respect to ash-concentration intervals in order to analyze the error trends within each class. The average rms error (rmse) values are about 0.04, 0.5, and 2.2 g/m$^3$ for fine ash, coarse ash and lapilli, respectively, and are relatively independent of concentration regime. For low values of ash concentration (below the ash class rmse), the percentage error may be larger than 100% as expected, whereas the structure of rmse with respect to $C_a$ reflects the Gaussian random generation of synthetic ash classes. If we compare these results with those obtainable by using an error budget neglecting the particle-combination uncertainty in (18), we would obtain a reduced estimate variance as expected.

## III. Subglacial Eruption Case Study

The eastern region of Iceland has been characterized by an increased earthquake activity in the last decade [24]–[26]. Hazards arising from subglacial volcanism are due mainly to the explosive effects of magma–ice interaction, which generates a tephra-laden plume of steam that ascends rapidly into the upper atmosphere. This scenario can pose a severe and widespread

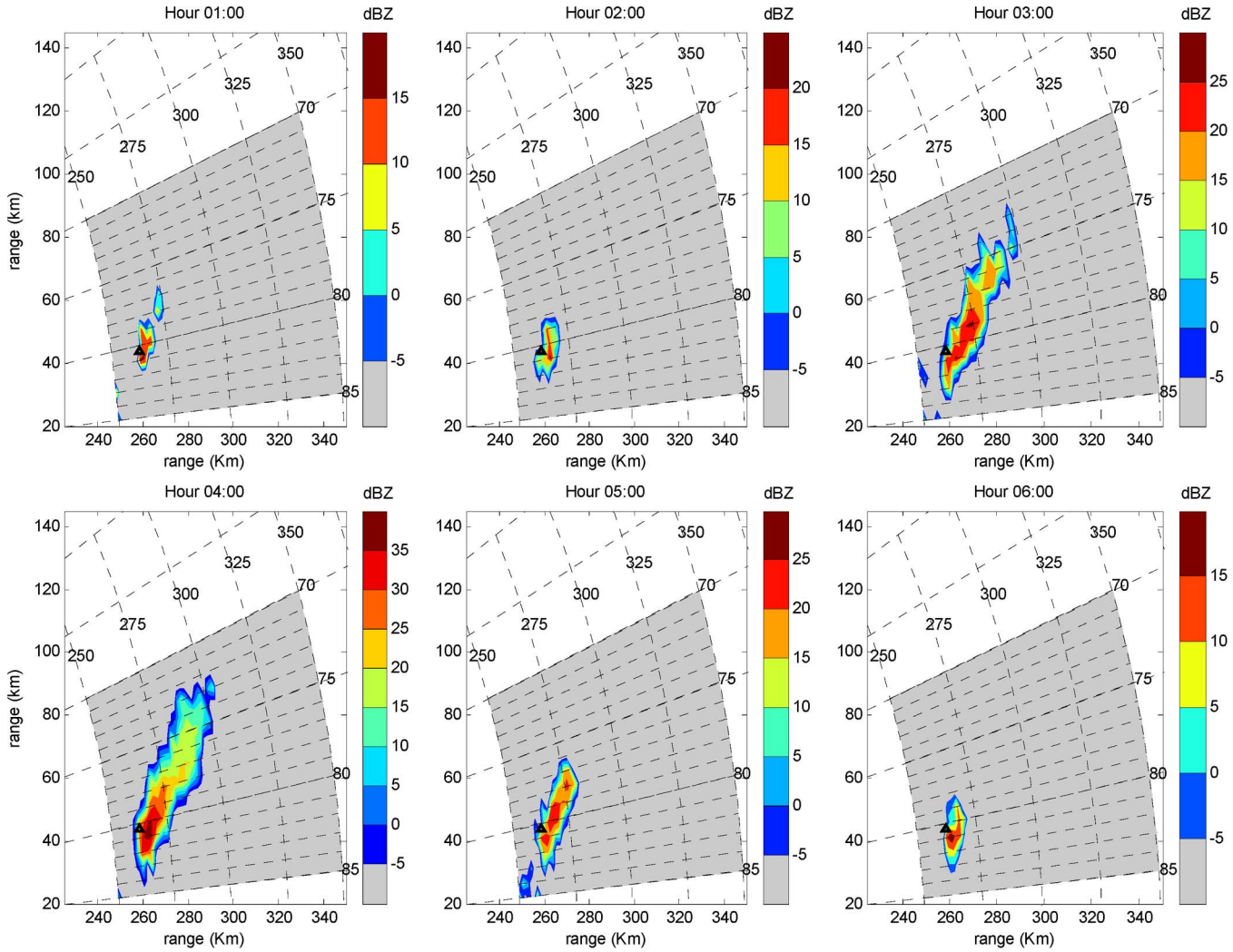


Fig. 5. PPI radar images of the subglacial volcanic eruption of Grímsvötn at 0.5° elevation angle on November 2, 2004. (Top panels) PPIs from 01:00 to 03:00 UTC. (Bottom panels) PPIs from 04:00 to 06:00 UTC.

risk to aviation. The melted ice can also lead to catastrophic outburst floods, known by the Icelandic term "jökulhlaup." They are a severe hazard along affected rivers with the potential to devastate populated areas.

Grímsvötn is one of the most active volcanoes in Iceland, with an $\sim 62$ km$^2$ caldera covered by 150- to 250-m-thick ice. Its highest peak Grímsfjall, on the southern caldera rim, reaches an elevation of 1722 m (e.g., [15] and [20]). Volcanic eruptions, numbering several per century, are phreato-magmatic because of the ice cover, and they usually persist for days to weeks. Geothermal activity continuously melts the overlying ice, and meltwater accumulates in a subglacial lake within the caldera until the surrounding ice is breached. Volcanic eruptions in Grímsvötn often coincide with jökulhlaups.

### *A. Time Evolution of Grímsvötn Subglacial Eruption*

In the morning of November 1, a jökulhlaup tremor was observed on the seismic records at the Grímsfjall station. The Grímsvötn eruption started in the evening of November 1, 2004 and was observed by a C-band weather radar located in Keflavik, Iceland [20]. The first plume detected by the Keflavik radar was at 23:05 Universal Time Coordinate (UTC) on November 1, 2004. Lightning over Grímsvötn, which accompanied the rising plume, was eventually seen at about 03:00 UTC, but darkness and weather conditions prevented visual observation of the eruption site. The eruption in the night of November 2 was followed by frequent plumes, and the last one, detected by the weather radar, was at 08:30 UTC in November 3. After this time, the plume was too low to be detected by the radar (reaching 6 km height or less). The Icelandic Meteorological Office (IMO) received information from local observers on the site, saying that, from approximately 16:00 UTC in November 3, the plume only reached up to about 150–200 m height. In the morning of November 4 (approximately at 10:00 UTC), IMO got information on site that the plume reached up to 1 to 2 km height. As of November 3, there was a visual estimate and might be off by some hundreds of meters. The eruption gradually ceased after that and declared finished in November 7.

Meteorological observations and synoptic analysis show that in November 1, a low-pressure system was moving toward west of Iceland from the south. In November 2 at 00 UTC, the low-pressure system was west of Iceland, which

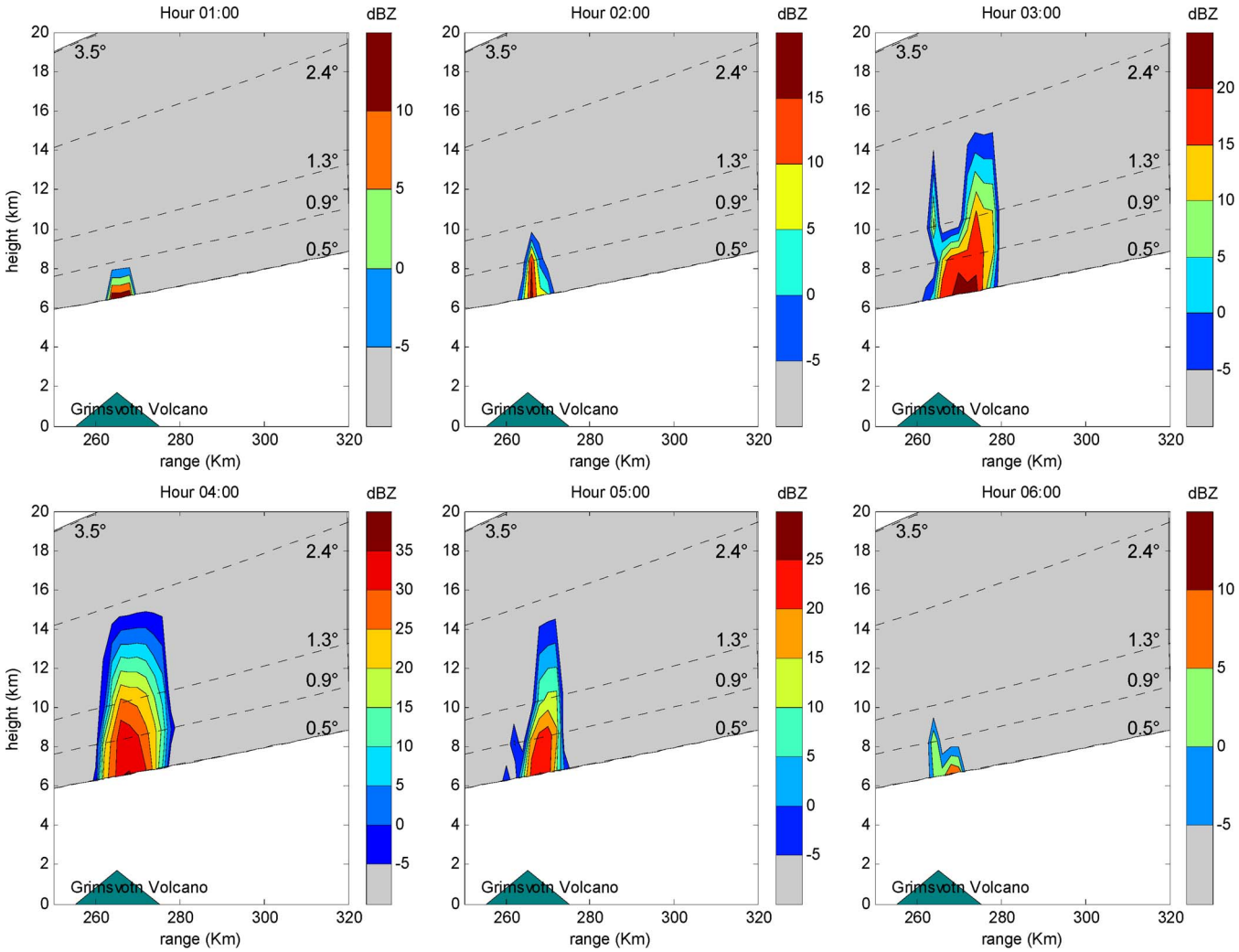


Fig. 6. Same as in Fig. 5, but for the RHI radar sections along the line of sight linking the Keflavik radar and the Grímsvötn volcano vent about 265 km long. The volcano vent is indicated by a triangle.

led to strong southerly and south–southwesterly winds over Iceland. A rawinsonde was launched at 00 UTC and 12 UTC from the Keflavík synoptic meteorological station in Iceland. Those measurements showed that the wind from the surface up to approximately 15 km height was southerly to south–southwesterly in November 1 until November 3 at 12:00 UTC. Temperatures at the surface were between $+5^\circ$ to $+10\,^\circ$C and freezing level between 1200 to 1500 m height.

During the most active phase of the volcano, i.e., from the time the volcanic plume reached the surface, detected by the radar at 23:05 UTC in November 1 until midday of November 3, the main wind direction was from the south and southwest from the surface up to approximately 15 km height. Hence, the plume blew to the north and northeast.

### B. Radar Imagery

The Keflavik weather radar is a C-band radar without a Doppler capability, located about 3 km north of the Keflavik international airport at 47 m above sea level in southwest Iceland and operated by IMO. Its main operational characteristics are a transmitted peak power $P_t$ of 245.2 kW, an antenna beamwidth of 0.9°, a pulse duration of 2.15 $\mu$s, a pulse repetition frequency of 250 Hz, and an antenna gain of 44.9 dB. Scanned images are routinely acquired every 20 min for normal weather monitoring and every 5 min during volcanic eruptions. A single-polarized microwave weather is able to detect the measured average backscattered power $P_r$ at range $r$ and convert it into measured horizontally polarized radar reflectivity (factor) $Z_{Hm}$. For ash monitoring at microwaves below 20 GHz, the path attenuation factor $L_H$, due to particle and gas absorption along the ray, is usually equal to about one.

Radar volume scans were continuously acquired, and data have been made available from 23:00 on November 1, 2004 until 06:00 UTC on November 2, 2004 every half an hour. Reflectivity data were radially averaged to 2 km in order to increase the measurement sensitivity (equal to about $-5$ dBZ around the 260-km range). Considering a distance of about 260 km between the Keflavik radar and the Grímsvötn volcano, volcanic ash clouds can be detected at heights higher than about 6 km using the minimum elevation of 0.5°. This means that the volcanic eruption cloud cannot be detected between the Grímsvötn summit at 1725 and 6000 m altitude. By comparing this range with the expected freezing level (around 1350 m)

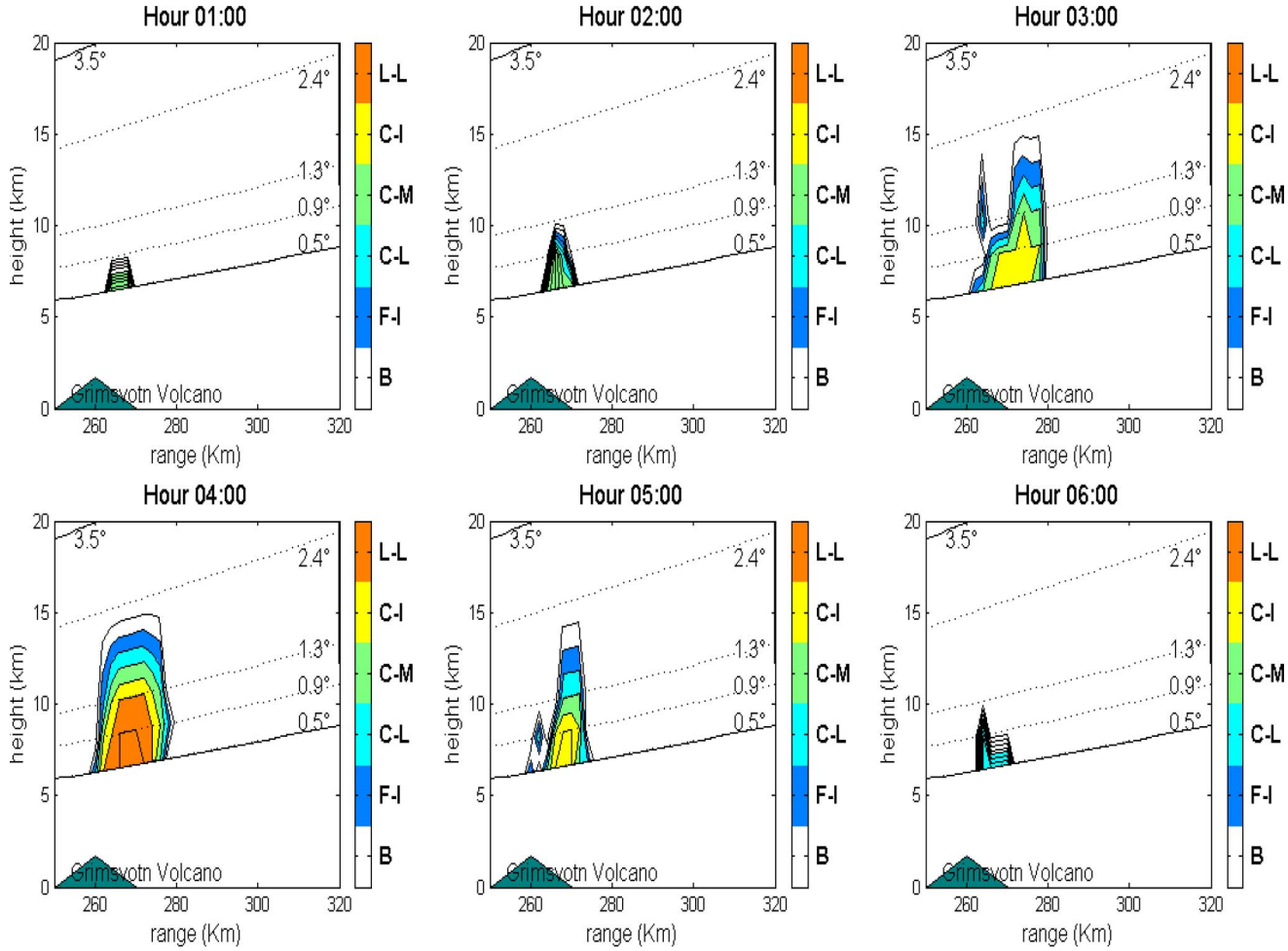


Fig. 7. As in Fig. 6, but for the estimated ash classes. (F-I) Fine ash with intense concentration. (C-L) Coarse ash with light concentration. (C-M) Coarse ash with moderate concentration. (C-I) Coarse ash with intense concentration. (L-L) Lapilli with light concentration. (B) Background clear air.

and considering the phreato-magmatic nature of Grímsvötn eruptions, we may expect the formation of ice particles and combination processes within the ash plume, such as ice nucleation around ash nuclei. Since we cannot discriminate ice–ash aggregation from pure ash clouds using a single-polarization radar, we can adopt the conservative model in (17) to include this uncertainty in our classification and retrieval algorithm given in (18) and (19).

Fig. 5 shows the time sequence of the plan position indicators (PPIs), acquired by the Keflavik radar between 01:00 and 06:00 UTC at 0.5° elevation every hour. The same is shown in Fig. 6, but for the range height indicators (RHIs) along the line of sight linking the Keflavik radar and the Grímsvötn volcano vent between 0.5° and 3.5° elevation angles. All ground clutter echoes and precipitation signatures below 3 km have been properly cancelled.

The signal of volcanic cloud is quite evident from both PPI and RHI signatures with values up to 40 dBZ around 04:00 UTC. The advection of the volcanic plume toward northwest is easily detectable from PPI sequence and the reflectivity maximum contour results to be slightly displaced with respect to the volcano. From the PPI and RHI radar imagery, we can derive the extension of the ash-cloud area, which is about 1000 km$^2$ with an advection wind velocity of about 90 km/h at the time of its maximum development around 04:00 UTC.

### C. Volcanic Cloud Ash Retrieval

The measured reflectivity imagery can be inverted to retrieve the ash class, ash concentration, and ashfall rate by applying the VARR technique basically expressed in (18) and (19). From the environmental conditions described in Section II-A, it is reasonable to assume that the ash eruption took place above the freezing level. This means that, if cloud hydrometeors are formed and eventually aggregated with ash particles, the water particles are basically frozen. If the VARR classification algorithm is applied, from radar RHI data, we can detect the class index, as shown in Fig. 7. As a further step, Figs. 8 and 9 show the results in terms of estimated ash concentration $C_a$ and fall-rate $R_a$, obtained by applying the VARR technique to the measured reflectivity RHI data.

Within a sub-Plinian eruption, lapilli can be suspended in air for some hours after the explosion. A size sorting of ash particles is also typical during the evolution of the erupted volcanic cloud [27]. The ash class spatial distribution in Fig. 7 closely follows the evolution of the radar reflectivity RHI. At the early stage, fine and coarse ashes are present with light-to-moderate concentrations. During the maximum extension and eruption peak around 04:00 UTC, a light concentration of lapilli is detected, slightly shifted with respect to the volcano vent. Indeed, this shift is already present at the early stage around

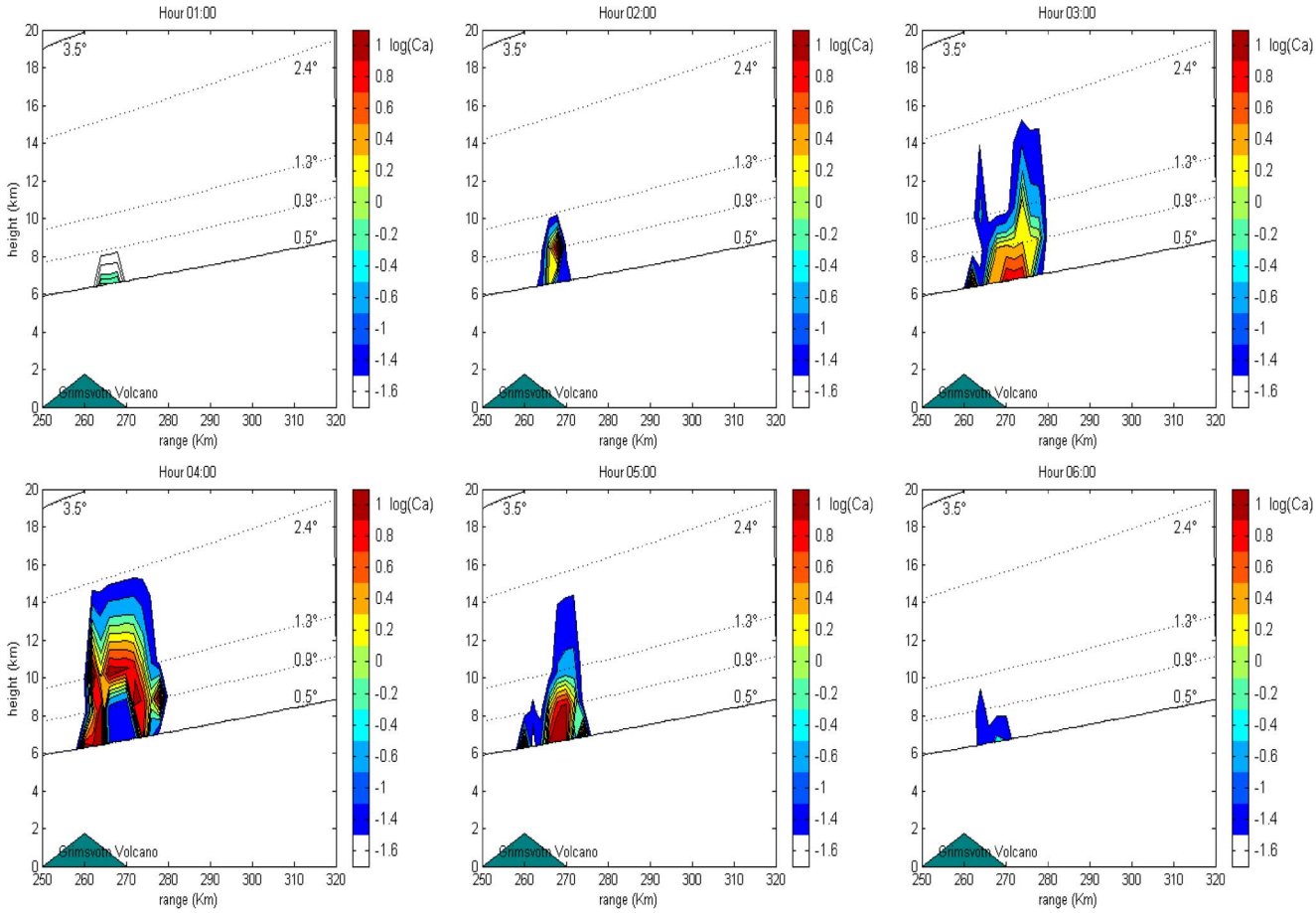


Fig. 8. As in Fig. 7, but for the estimated ash concentration $C_a$ (in grams per cubic meter) expressed in $\log_{10}[C_a]$ for plot convenience.

01:00 UTC, denoting the significant wind advection. Indeed, around 05:00, a lower fine-ash plume emerges within the radar visibility cone in a position closer to the volcano vent. Fine ash is weakly detected at the borders of RHI radar sector. Around 06:00 UTC, the volcanic ash cloud has almost completely fallen and is going to be dispersed as a near-surface ash plume with small concentration, as documented in Section III-A.

Fig. 8 shows the time evolution of ash-concentration spatial distribution RHI. The spatial pattern of estimated $C_a$ does not strictly resemble that of radar reflectivity in Fig. 6. This is due to that fact that a given reflectivity may be due either to a low concentration of bigger particles or to a high concentration of smaller particles [16]. By applying VARR classification, we can address this ambiguity by recognizing the regions of fine, coarse, and large ash particles. This is particularly evident at 04:00 UTC, where the low amount of lapilli, causing high radar reflectivity, is contiguous to regions of large amount of coarse ash particles.

Fig. 9 shows the time sequence of the estimated ashfall flux RHI. This estimate is dependent on the velocity–diameter law used to convert mass into fluxes, as from (6). Here, we used the power law derived from the data of Mt. St. Helens eruption in 1980 with $w_u = 0$ in (6) [11], [15]. The spatial pattern of estimated $R_a$ resembles that of estimated $C_a$. If a uniform ash flux is assumed to be between the lowest visible radar bin and the surface (in our case, about 4 km), then the ashfall at ground might be computed during the whole event. This ashfall estimate might be directly compared with the available ground measurements of ash deposits. Unfortunately, in this case study, we do not have any chance to verify these results.

## IV. Conclusion

The potential of using a ground-based C-band weather radar system for volcanic ash-cloud detection and quantitative retrieval has been evaluated. An application of the physically based VARR inversion technique has been shown, taking into consideration the eruption of the Grímsvötn volcano in Iceland in November 2004. Volume scan data from a Doppler C-band radar, located at 260 km from the volcano vent, have been processed by means of VARR. Examples of the achievable VARR products have been commented and discussed. The case study has been analyzed in terms of its evolution by looking at both radar measurements and ash products, derived from the measurements themselves. The analysis has clearly shown the unique features of radar remote sensing of sub-Plinian volcanic eruptions.

We have also evaluated and incorporated the possible effects of nonprecipitating hydrometeors within the VARR approach. The coexistence and mixture of ash particles with cloud ice and water droplet generally lead to a reduction of the measured reflectivity up to 5–10 dBZ for a fractional combination of

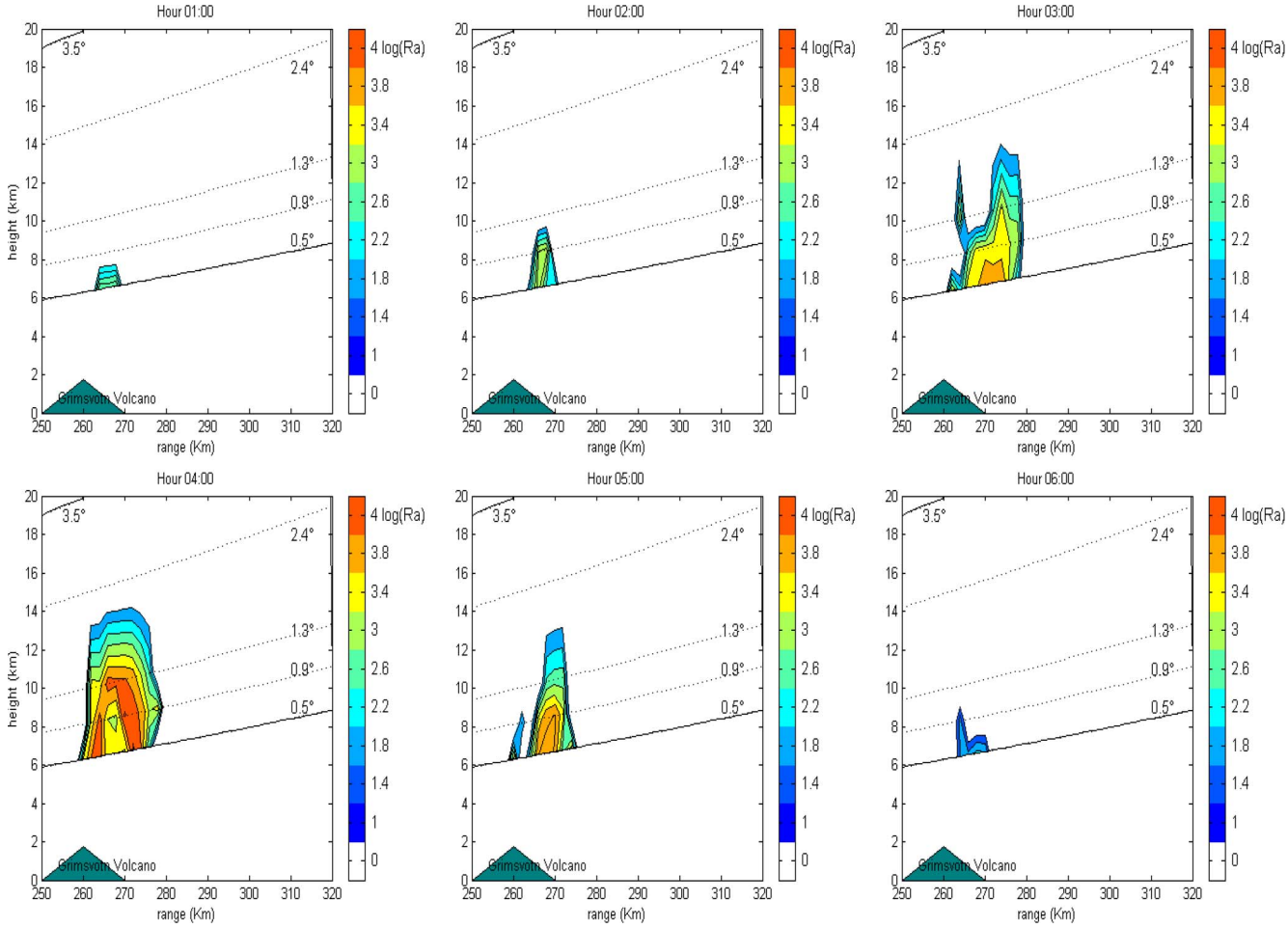


Fig. 9. As in Fig. 7, but for the estimated ashfall rate $R_a$ (in kilograms per square meter per steradian) expressed in $\log_{10}[R_a]$ for plot convenience.

about 50%. Since, by using a single-polarization weather radar, we do not have any chance to discriminate between ash, hydrometeors, and mixed particles, we have included the particle-combination uncertainty within the inversion scheme, dealing with the increase of the estimation error variance.

For future developments, we might resort to dual-polarized weather radar capable of measuring polarimetric observables, both in amplitude and phase. If these polarimetric radar data were available during a volcanic eruption, significant improvements of the obtained retrievals could be achieved by taking into account not only the particle composition but also their shape. In this respect, weather radar at X-band might even show a better sensitivity with respect to the corresponding C-band systems having the same characteristics. Finally, a portable weather radar system might overcome the limitation of observing a volcanic eruption from far distances, as in the case study here considered.

The ground validation of radar-based ash estimates remains the major problem of this proposed observation technique. Unfortunately, *in situ* validation is not an easy task due to the difficulty to automatically collect ash deposits on the surface (in a way similar to rain gauges for rainfall) and to penetrate through ash plumes by aircraft (in a way similar to airborne sampling through rainstorms). Indeed, optical disdrometers may be used to measured ash PSD and fluxes at ground, using the same techniques to sample raindrop sized distributions. A proper design and deployment of an ash disdrometer network around active volcanoes, coupled with a portable microwave radar, could lead to new insights and final assessments of volcanic ash-cloud radar remote sensing.

## ACKNOWLEDGMENT

The authors would like to thank Dr. R. Hannesen (Selex-Gematronik, Germany) and to Dr. P. Crochet (Iceland Meteorological Office, Iceland) for providing the radar data, Dr. G. Vulpiani and Dr. G. Ferrauto of the Centro di Eccellenza per l'integrazione di Tecniche di Telerilevamento e Modellistica Numerica per la Previsione di Eventi Meteorologici Severi, University of L'Aquila, L'Aquila, Italy, for their contributions, and the anonymous reviewer for the detailed and useful comments.

## REFERENCES

[1] R. S. J. Sparks, M. I. Bursik, S. N. Carey, J. S. Gilbert, L. Glaze, H. Sigurdsson, and A. W. Woods, *Volcanic Plumes*. New York: Wiley, 1997.

[2] G. A. Valentine and K. H. Wohletz, "Numerical models of Plinian columns and pyroclastic flows," *J. Geophys. Res.*, vol. 94, pp. 1867–1887, 1989.

[3] H. F. Graf, M. Herzog, J. M. Oberhuber, and C. Textor, "The effect of environmental conditions on volcanic plume rise," *J. Geophys. Res.*, vol. 104, no. D20, pp. 24 309–24 320, Oct. 1999.

[4] L. Wilson, "Explosive volcanic eruptions—II. The atmospheric trajectories of pyroclasts," *Geophys. J. Int.*, vol. 30, no. 4, pp. 381–392, Dec. 1972.
[5] A. B. Clarke, B. Voight, A. Neri, and G. Macedonio, "Transient dynamics of vulcanian explosions and column collapse," *Nature*, vol. 415, no. 6874, pp. 897–901, Feb. 2002.
[6] T. J. Casadevall, "Volcanic ash and aviation safety," *U.S. Geol. Surv. Bull.*, vol. 2047, pp. 450–469, 1994.
[7] W. I. Rose, D. Delene, D. Schneider, G. Bluth, A. Krueger, I. Sprod, C. McKee, H. Davies, and G. Ernst, "Ice in the 1994 Rabaul eruption cloud: Implications for volcano hazard and atmospheric effects," *Nature*, vol. 375, no. 6531, pp. 477–479, Jun. 1995.
[8] S. Wen and W. I. Rose, "Retrieval of sizes and total masses of particles in volcanic clouds using AVHRR bands 4 and 5," *J. Geophys. Res.*, vol. 99, no. D3, pp. 5421–5431, 1994.
[9] N. Krotkov, D. Flittner, and A. Krueger, "Effect of particle non-sphericity on satellite monitoring of drifting volcanic ash clouds," *J. Quant. Spectrosc. Radiat. Transf.*, vol. 63, no. 2–6, pp. 613–630, Sep. 1999.
[10] W. I. Rose, G. J. S. Bluth, and G. G. J. Ernst, "Integrating retrievals of volcanic cloud characteristics from satellite remote sensors: A summary," *Philos. Trans. R. Soc. London A, Math. Phys. Eng. Sci.*, vol. 358, no. 1770, pp. 1538–1606, 2000.
[11] D. M. Harris and W. I. Rose, "Estimating particle sizes, concentrations, and total mass of ash in volcanic clouds using weather radar," *J. Geophys. Res.*, vol. 88, no. C15, pp. 10 969–10 983, Dec. 1983.
[12] W. I. Rose, A. B. Kostinski, and L. Kelley, "Real time C band radar observations of 1992 eruption clouds from Crater Peak/Spurr Volcano, Alaska," *U.S. Geol. Surv. Bull.*, vol. 2139, pp. 19–26, 1995. (Spurr Eruption, edited by T. Keith).
[13] M. Maki, K. Iwanami, R. Misumi, R. J. Doviak, T. Wakayama, K. Hata, and S. Watanabe, "Observation of volcanic ashes with a 3-cm polarimetric radar," in *Proc. 30th Radar Meteorol. Conf.*, 2001, p. 5.13.
[14] C. Lacasse, S. Karlsdóttir, G. Larsen, H. Soosalu, W. I. Rose, and G. G. J. Ernst, "Weather radar observations of the Hekla 2000 eruption cloud, Iceland," *Bull. Volcanol.*, vol. 66, no. 5, pp. 457–473, Jul. 2004.
[15] F. S. Marzano, S. Barbieri, G. Vulpiani, and W. I. Rose, "Volcanic cloud retrieval by ground-based microwave weather radar," *IEEE Trans. Geosci. Remote Sens.*, vol. 44, no. 11, pp. 3235–3246, Nov. 2006.
[16] F. S. Marzano, G. Vulpiani, and W. I. Rose, "Microphysical characterization of microwave radar reflectivity due to volcanic ash clouds," *IEEE Trans. Geosci. Remote Sens.*, vol. 44, no. 2, pp. 313–327, Feb. 2006.
[17] M. Herzog, H. F. Graf, C. Textor, and J. M. Oberhuber, "The effect of phase changes of water on the development of volcanic plumes," *J. Volcanol. Geotherm. Res.*, vol. 87, no. 1–4, pp. 55–74, Dec. 1998.
[18] G. Veitch and A. W. Woods, "Particle aggregation in volcanic eruption columns," *J. Geophys. Res.*, vol. 106, no. B11, pp. 26 425–26 441, 2001.
[19] C. Textor, H. G. Graf, M. Herzog, J. M. Oberhuber, W. I. Rose, and G. G. J. Ernst, "Volcanic particle aggregation in explosive eruption columns. Part I: Parameterization of the microphysics of hydrometeors and ash," *J. Volcanol. Geotherm. Res.*, vol. 150, no. 4, pp. 359–377, Feb. 2006.
[20] K. S. Vogfjörd, S. S. Jakobsdóttir, G. B. Gudmundsson, M. J. Roberts, K. Ágústsson, T. Arason, H. Geirsson, S. Karlsdóttir, S. Hjaltadóttir, U. Ólafsdóttir, B. Thorbjarnardóttir, T. Skaftadóttir, E. Sturkell, E. B. Jónasdóttir, G. Hafsteinsson, H. Sveinbjörnsson, R. Stefánsson, and T. V. Jónsson, "Forecasting and monitoring of subglacial eruption in Iceland," *EOS, Trans. Amer. Geophys. Union*, vol. 86, no. 26, pp. 245–252, Jun. 2005.
[21] F. T. Ulaby, R. K. Moore, and A. K. Fung, *Microwave Remote Sensing: Active and Passive*, vol. 1. Reading, MA: Addison-Wesley, 1982.
[22] H. Sauvageot, *Radar Meteorology*. Norwood, MA: Artech House, 1992.
[23] C. D. Rogers, "Retrieval of atmospheric temperature and composition from remote measurement of thermal radiation," *Rev. Geophys. Space Phys.*, vol. 14, no. 4, pp. 609–624, Nov. 1976.
[24] M. T. Gudmundsson, F. Sigmundsson, and H. Bjornsson, "Ice–volcano interaction of the 1996 Gjalp subglacial eruption, Vatnajokull, Iceland," *Nature*, vol. 389, no. 6654, pp. 954–957, Oct. 1997.
[25] H. Björnsson, "Subglacial lakes and jökulhlaups in Iceland," *Glob. Planet. Change*, vol. 35, no. 3, pp. 255–271, Feb. 2002.
[26] E. Sturkell, P. Einarsson, F. Sigmundsson, S. Hreinsdottir, and H. Geirsson, "Deformation of Grimsvotn volcano, Iceland: 1998 eruption and subsequent inflation," *Geophys. Res. Lett.*, vol. 30, no. 4, p. 1182, Feb. 2003. DOI:10.129/2002GL016460.
[27] K. H. Wohletz, M. F. Sheridan, and W. K. Brown, "Particle size distributions and the sequential fragmentation/transport theory applied to volcanic ash," *Geophys. Res. Lett.*, vol. 16, pp. 15 703–15 721, 1989.

**Frank Silvio Marzano** (S'89–M'99–SM'03) received the Laurea degree (*cum laude*) in electrical engineering and the Ph.D. degree in applied electromagnetics from the University "La Sapienza" of Rome, Rome, Italy, in 1988 and 1993, respectively.

In 1993, he collaborated with the Institute of Atmospheric Physics, Consiglio Nazionale delle Ricerche, Rome. From 1994 to 1996, he was with the Italian Space Agency, Rome, as a Postdoctorate Researcher. After being a Lecturer with the University of Perugia, Perugia, Italy, in 1997, he is with the Department of Electrical Engineering and the Centro di Eccellenza per l'integrazione di Tecniche di Telerilevamento e Modellistica Numerica per la Previsione di Eventi Meteorologici Severi, University of L'Aquila, L'Aquila, Italy, coordinating the Satellite and Radar Remote Sensing Laboratory. Since 2005, he has been with the Department of Electronic Engineering, University "La Sapienza" of Rome, where he currently teaches courses on antennas, propagation, and remote sensing. His current research concerns passive and active remote sensing of the atmosphere from ground-based, airborne, and spaceborne platforms, with a particular focus on precipitation using microwave and infrared data, development of inversion methods, radiative transfer modeling of scattering media, and radar meteorology issues. He is also involved on radio propagation topics in relation to incoherent wave modeling, scintillation prediction, and rain fading analysis along satellite microwave links.

Dr. Marzano was the recipient of the Young Scientist Award of XXIV Union Radio Scientifique Internationale General Assembly in 1993 and the Alan Berman Research Publications Award from the Naval Research Laboratory, Washington, DC, in 1998. He has been acting as an Associated Editor of the IEEE GEOSCIENCE REMOTE SENSING LETTERS since January 2004. Since 2001, he has been an Italian National Delegate for the European Cooperation in the field of Scientific and Technical Research actions 720, 280, ES0702 and IC0802.

**Stefano Barbieri** received the Laurea degree in electronic engineering from the University "La Sapienza" of Rome, Rome, Italy, in 2005.

In 2005, he joined the Department of Electronic Engineering, University "La Sapienza" of Rome, to cooperate on radar remote sensing of volcanic ash clouds. He is also with the Centro di Eccellenza per l'integrazione di Tecniche di Telerilevamento e Modellistica Numerica per la Previsione di Eventi Meteorologici Severi, University of L'Aquila, L'Aquila, Italy.

**Errico Picciotti** received the Laurea degree (*cum laude*) in electrical engineering from the University of Ancona, Ancona, Italy, in 1992.

In 1997, he was with the Science and Technology Park of Abruzzo, L'Aquila, Italy, as a Radar Meteorologist. In 2002, he was a Researcher with the Centro di Eccellenza per l'integrazione di Tecniche di Telerilevamento e Modellistica Numerica per la Previsione di Eventi Meteorologici Severi, University of L'Aquila, L'Aquila, Italy, where he worked on radar systems and polarimetry. Since 2007, he has been with HIMET, L'Aquila, where he is the Coordinator of the Radar Meteorology Division.

**Sigrùn Karlsdóttir** received the Dr.Sc. degree in meteorology, with specialization in atmospheric chemistry, from the University of Oslo, Oslo, Norway, in 2000.

Since July 2000, she has been with the Icelandic Meteorological Office, where she led the Forecasting Division from 2004 to 2008 and has been the Chief Project Manager of natural hazards since 2009. She has been involved with different tasks related to meteorology, volcanic eruptions, and distribution of ash clouds.